Depletion Kinetics of Chromium Atoms by Sulfur Dioxide

Roy E. McClean

Chemistry Department, United States Naval Academy, Annapolis, Maryland 21402

Received: March 23, 2000; In Final Form: July 19, 2000

The gas-phase depletion kinetics of Cr(a^7S_3, a^5S_2, a^5D_J) in the presence of SO_2 are reported. Chromium atoms were produced by the 248 nm photodissociation of chromium carbonyl and were detected by laser-induced fluorescence. The ground state of Cr, a^7S_3, was found to react rapidly via a termolecular mechanism with SO_2. At 297 K, the limiting low-pressure third-order rate constant is $k_o = (2.68 \pm 0.41) \times 10^{-28}$ cm^6 molecule^{-2} s^{-1}, and the limiting high-pressure second-order rate constant is $k_\infty = (2.73 \pm 0.38) \times 10^{-10}$ cm^3 molecule^{-1} s^{-1}; the uncertainties represent $\pm 1\sigma$ in precision. k_o was found to decrease with increasing temperature. The binding energy of $CrSO_2$ is estimated at 53 kcal mol^{-1} from combining the kinetic results with unimolecular rate theory and density functional theory. Cr(a^5S_2) depleted with a rate constant of $k = 6.32 \times 10^{-10}$ cm^3 molecule^{-1} s^{-1}, and the a^5D_J spin/orbit states depleted at the collision rate of 2.97×10^{-10} cm^3 molecule^{-1} s^{-1}; overall uncertainties are estimated at $\leq 35\%$. Both chemical and physical quenching are likely for the excited states. The present work completes a study on the depletion kinetics of group 6 transition metal atoms by SO_2. Results are interpreted in terms of long-range attractive forces between Cr and SO_2 and the orbital occupancies of the Cr atomic states.

Introduction

Many gas-phase reactions involving both ground-state and excited-state transition metal (TM) atoms with SO_2 have been observed to proceed with little or no barriers.[1−7] In some cases, the relatively fast rates have been attributed to an electron-transfer mechanism whereby an electron is transferred from the TM atom to the SO_2. This mechanism is similar to the harpoon model used to explain the rapid rates observed for main group metal atoms reacting with halogen molecules.[8] Some TM/SO_2 systems proceed at rates greater than the collision rate, thus lending support for such a mechanism.[3] Due to the relatively large ionization potentials of TM atoms,[9] valence interactions are expected to play a role in their interactions with SO_2; i.e., the electron transfer occurs within the collision cross section and thus, energy barriers may be encountered. These barriers are likely due to the orbital occupancies of the TM atoms. TM atoms having $d^{n-1}s^1$ orbital occupancies, where n is the number of valence electrons, have generally been found to be more reactive than TM atoms having $d^{n-2}s^2$ orbital occupancies. Most of the TM/SO_2 systems that have been reported proceed through O atom abstraction channels.[1−7] In such reactions, it is the s^1 configuration that orbitally correlates with the transition metal oxides.[10]

Association reactions might also be consistent with the orbital occupancy argument. Adduct formation is the only accessible channel for ground-state Mn ($3d^54s^2$ $a^6S_{5/2}$) and ground-state Ni ($3d^84s^2$ a^3F_4) to react with SO_2 at relatively low temperatures.[11] Mn is unreactive toward SO_2. The first state of Mn with an s^1 configuration lies 17 053 cm^{-1} above the ground state[12] and, thus, is unaccessible at relatively low temperatures. The ground state of Ni is separated from the $3d^94s^1$ a^3D_3 state by only 205 cm^{-1} and has been found to react with SO_2 between 296 and 623 K. In fact, both Ni states react with SO_2 with identical rate constants. The electron-transfer mechanism cannot account for the large difference in reactivities between Mn and Ni because Mn has a smaller ionization potential than Ni.[9]

In this paper, we report the association reaction of ground-state Cr with SO_2,

$$Cr + SO_2 + M \rightarrow CrSO_2 + M \qquad (1)$$

where M is a third body. This work was performed to experimentally determine if the orbital occupancy trend is also prevalent in association reactions involving TM atoms and SO_2. Density functional theory (DFT)[13] and Troe's factorization method[14] are combined with the kinetic results to estimate the binding energy of the $CrSO_2$ adduct. The depletion kinetics of several excited states of Cr of both s^1 and s^2 occupancies have also been investigated. The results on the Cr + SO_2 system are discussed in the greater context of group 6 + SO_2 systems. (The Cr + SO_2 reaction has previously been reported; however, this work was performed under shock tube conditions where the temperature was 1000−3000 K.[15])

Experimental Section

Details of the experimental arrangement have been described in detail elsewhere[16] and are only summarized here. The laser photolysis/laser-induced fluorescence (LP/LIF), slow-flow technique was used in this work.

The reaction chamber was a stainless steel cross with gas inlet and outlet ports, a viewport for LIF detection, and windows for passage of the laser beams; the chamber was contained in a convection oven capable of attaining temperatures up to 628 K. Chromium carbonyl, the chromium precursor, was entrained in a slow flow of argon gas. The argon buffer gas, diluted precursor, and SO_2 passed through separate mass flow controllers, after which they combined into one line and flowed slowly through the reaction chamber. A slow flow of argon also passed over the windows in order to minimize the deposition of the precursor and photofragments. Total flows were between 150 and 8500 sccm, depending on the total pressure. Partial pressures of the individual components were determined by their relative

10.1021/jp001101m
Published on Web 09/06/2000

TABLE 1: Atomic States of Cr and LIF Information

Cr state[a]	energy (cm^{-1})	λ (nm) of excitation[b]	detection filter
a^7S_3	0.00	360.532	350 nm, 100 nm fwhm
a^5S_2	7593.16	454.595	450 nm, 50 nm fwhm
a^5D_o	7750.78	389.404	400 nm, 50 nm fwhm
a^5D_1	7810.82	391.625	400 nm, 50 nm fwhm
a^5D_2	7927.47	392.103	400 nm, 50 nm fwhm
a^5D_3	8095.21	392.865	400 nm, 50 nm fwhm
a^5D_4	8307.57	391.917	400 nm, 50 nm fwhm

[a] Reference 12. [b] Reference 17.

flow rates and the total pressure in the reaction chamber. Pressures were measured by Baratron manometers and temperatures were measured with a thermocouple attached to the reaction chamber.

Chromium atoms were produced from $Cr(CO)_6$ by the unfocused output of an excimer laser operating on KrF (248 nm) at 21 Hz. Rate constant measurements did not depend on the photolysis fluences, which were approximately 200−400 mJ cm^{-2} in the reaction chamber. Detection of chromium atoms was by LIF using laser light from an excimer-pumped dye module. The photolysis and dye beams counterpropagated through the chamber. Neutral density filters were used to ensure that the dye laser fluence (less than 1 mJ/pulse) did not affect the kinetic results. A photomultiplier tube and lens focusing system, situated 90° to the laser beams, collected the LIF signal, which was subsequently sent to a gated boxcar sampling module, and the boxcar's output was stored and analyzed by a computer. The Cr states studied and the corresponding excitation wavelengths are listed in Table 1.[12,17]

All kinetic results are based on the disappearance of Cr atoms under pseudo-first-order conditions where the number density of Cr was much less than the number density of SO_2 and Ar. Reaction time was taken as the delay time between the laser pulses. For a given experimental run, the delay time was varied by a digital delay generator controlled by a computer. Minimum delay times were typically 1−10 μs in order to prevent overlap of the prompt emission from photolysis products with the LIF signal. The trigger source for these experiments was scattered pump laser light incident upon a fast photodiode. LIF decay traces consisted of 200−500 points, each point averaged over 2−10 laser shots. LIF intensities were proportional to Cr atom number densities.

Materials. The following substances were used as received: $Cr(CO)_6$ (Aldrich, 99%), Ar (Potomac Airgas, Inc., 99.9998%), SO_2 (MG Industries, 99.98%).

Data Analysis and Results

The production of the Cr states studied in this work (see Table 1) from $Cr(CO)_6$ requires a two-photon dissociation process at 248 nm.[18,19] A two-photon process can also produce other fragments. We detected LIF from the spin−orbit states of the a^5G_J term in the vicinity of 452.6−454.6 nm; these states lie at ≈20 521 cm^{-1}. There was no indication that the a^5G_J spin−orbit states and other photofragments interfered with the decay kinetics of $Cr(a^7S_3)$ and $Cr(a^5D_{1-4})$ in the presence of SO_2. However, slight nonexponential temporal behavior was observed for $Cr(a^5S_2)$ and $Cr(a^5D_0)$ in the presence of SO_2. This observation is discussed below.

$Cr(a^7S_3)$. A typical exponential decay trace is shown in Figure 1. The trace represents the decay of $Cr(a^7S_3)$ in the presence of added SO_2 at 297 K and 200 Torr total pressure. Partial pressures of the precursor $Cr(CO)_6$ are not accurately known in these experiments. However, based on the carrier flow rate and pressure, total flow rate, and total pressure, chromium carbonyl's partial pressure in the reaction chamber is estimated to be less than 0.5 mTorr for all experiments. Only a small fraction of $Cr(CO)_6$ is dissociated and, therefore, pseudo first-order decay kinetics are maintained. The solid line through the data is an exponential fit to the equation

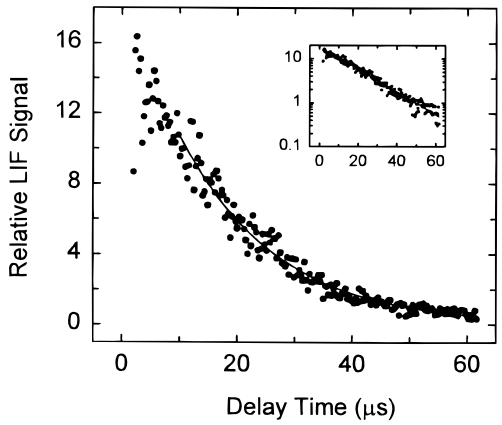

Figure 1. Typical decay profile of Cr in the presence of SO_2. Data are for $Cr(a^7S_3)$. $T = 297$ K, $P_{tot} = 200$ Torr, $P_{SO_2} = 11.0$ mTorr. The solid line through the data is an exponential fit with $\tau = 16.7$ μs. The inset is the same data in semilogarithmic form; note the linearity.

$$I = I_o \exp(-t/\tau) \quad (2)$$

where I and I_o are the LIF signals at time t and initial time for fitting, respectively, and τ is the lifetime from which the pseudo-first-order rate constant, $1/\tau$, is obtained. The data in Figure 1 are fitted from 10 to 60 μs. The 10 μs delay was chosen to avoid the slight growth in the LIF signal at relatively short delay times. The growth is attributed to collisional deactivation of higher energy states to the ground state. $1/\tau$ is given by

$$1/\tau = 1/\tau_o + k_{obs}[SO_2] \quad (3)$$

where τ_o is the lifetime of Cr without added SO_2, k_{obs} is the second-order rate constant, and $[SO_2]$ is the partial pressure of SO_2. τ_o represents the lifetime of Cr in the presence of species other than SO_2 in the reaction chamber, and the diffusion of Cr out of the detection zone. τ_o was usually long compared to τ. Second-order rate constants were obtained from the slopes of plots of $1/\tau$ vs SO_2 partial pressures, such as that shown in Figure 2. Note that the intercept ($1/\tau_o$) is relatively small so that interference from photofragments and diffusion were minimal.

The measured second-order rate constants are listed in Table 2. The uncertainties resulting from the linear regression fits such as that in Figure 2 were approximately 3% ($\pm 1\sigma$) in precision. The overall uncertainties for $Cr(a^7S_3)$, estimated at ±30% at the 95% confidence limit, include statistical scatter in the data, the reproducibility of k_{obs}, and instrumental uncertainties such as digital delay and flow measurements. As shown in Table 2, the second-order rate constants of $Cr(a^7S_3)$ increase with increasing total pressure and decrease with increasing temperature, an indication of the termolecular reaction mechanism

$$Cr + SO_2 \rightleftharpoons CrSO_2^* \quad (4)$$

$$CrSO_2^* + M \rightarrow CrSO_2 + M \quad (5)$$

The third body M was predominantly argon; the partial pressures of the other gaseous components were too low to contribute significantly to the stabilization of the $CrSO_2^*$ complex.

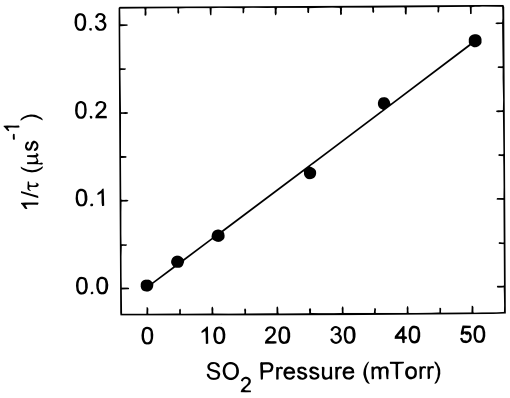

Figure 2. Typical plot for determining second-order rate constants. The conditions are the same as in Figure 1, except the partial pressures of SO_2 are changing. Each point represents an average of two to four measurements. The slope gives $k_{obs} = (1.71 \pm 0.05) \times 10^{-10}$ cm^3 molecule^{-1} s^{-1}, where the uncertainty is $\pm 1\sigma$ from the linear regression.

TABLE 2: Measured Second-Order Rate Constants for the Depletion of Cr by SO_2[a]

		k_{obs} (10^{-11} cm^3 molecule^{-1} s^{-1})	
state	P (Torr)	297 K	534 K
a^7S_3	5	2.87	
	10	5.49	
	20	7.23	
	50	11.4	2.90
	100	13.7	4.32
	200	17.1	5.68
	300	20.8	7.18
	400	22.1	7.72
	500	24.7	9.18
	600		9.30
a^5S_2	5−20	63.2	
a^5D_{0-4}	30	29.7	

[a] Buffer = argon. Overall uncertainties are ±30% at the 95% confidence limit, except for the a^5S_2 state, which are estimated at ±35%.

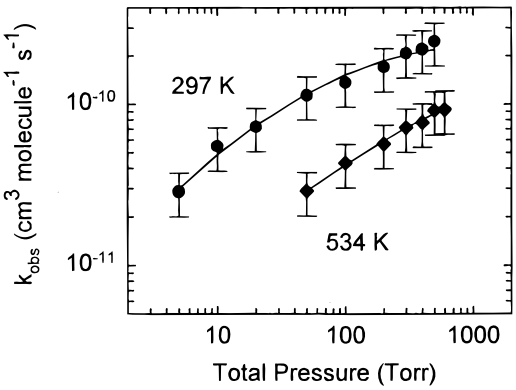

Figure 3. Pressure dependence of $Cr(a^7S_3) + SO_2$. The solid lines through the data are fits to eq 6. Error bars represent overall uncertainties of ±30%. See text for results of the fits.

Plots of the second-order rate constants as a function of total pressure are shown in Figure 3. The solid lines through the data are fits to Troe's formalism,[14]

$$\log k = \log \frac{k_o[M]}{1 + (k_o[M]/k_\infty)} + \frac{\log F_c}{1 + [\log(k_o[M]/k_\infty)]^2} \quad (6)$$

where k_o is the limiting low-pressure third-order rate constant, k_∞ is the limiting high-pressure second-order rate constant, [M] is the buffer gas number density, and F_c is the broadening factor. Results of the fits are

297 K:
$$k_o = (2.68 \pm 0.41) \times 10^{-28} \text{ cm}^6 \text{ molecule}^{-2} \text{ s}^{-1}$$
$$k_\infty = (2.73 \pm 0.38) \times 10^{-10} \text{ cm}^3 \text{ molecule}^{-1} \text{ s}^{-1}$$
$$F_c = 0.68 \pm 0.12$$

534 K:
$$k_o = (7.5 \pm 2.0) \times 10^{-29} \text{ cm}^6 \text{ molecule}^{-2} \text{ s}^{-1}$$
$$k_\infty = (1.68 \pm 0.21) \times 10^{-10} \text{ cm}^3 \text{ molecule}^{-1} \text{ s}^{-1}$$
$$F_c = 0.56 \pm 0.11$$

where the uncertainties represent $\pm 1\sigma$ in precision. k_∞ appears to decrease with increasing temperature. However, the relatively long extrapolations of the second-order rate constants to the high-pressure limit as the temperature increases and the combined uncertainties in k_∞ preclude an accurate assessment of this observation. Note, however, that k_∞ is on the order of the gas collision rate constant of $\approx 2.1 \times 10^{-10}$ cm^3 molecule^{-1} s^{-1}.[20-22]

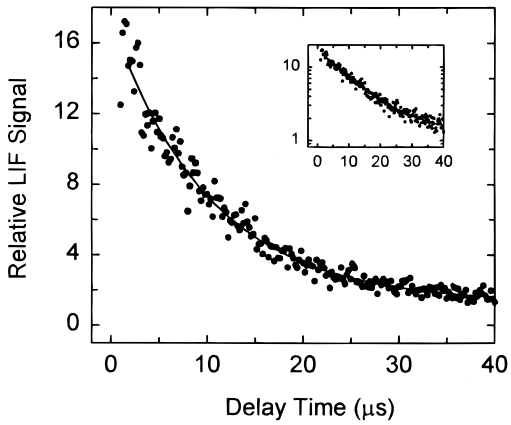

Figure 4. Decay profile of $Cr(a^5S_2)$ in the presence of SO_2. $T = 296$ K, $P_{tot} = 10$ Torr, $P_{SO_2} = 4.44$ mTorr. The solid line through the data is a fit to the equation $I = I_o \exp(-t/\tau) +$ constant; $\tau = 10.3$ μs. The inset is the same data in semilogarithmic form; note the nonexponential nature of the plot at relatively long times.

$Cr(a^5S_2) + SO_2$ was studied at 296 K at 5, 10, and 20 Torr total pressure. Nonexponential decay kinetics were observed, as shown in the example in Figure 4; note the nonlinearity in the inset beginning at ≈ 25 μs. The solid line through the data is a fit to the expression

$$I = A \exp(-t/\tau) + B \quad (7)$$

where A, B, and τ are fitted parameters. The nonexponential behavior is attributed to the depletion scheme

$$Cr^* \rightarrow Cr(a^5S_2) \quad (8a)$$

$$Cr(a^5S_2) \rightarrow \text{products} \quad (8b)$$

where Cr* is a Cr state lying higher in energy than $Cr(a^5S_2)$. The biexponential expression, $I = A \exp(-t/\tau_{8b}) + B \exp(-t/\tau_{8a})$, where A and B are related to the populations of Cr* and $Cr(a^5S_2)$, was also used to fit the data. The biexponential equation is more applicable to the decay scheme given by eqs 8a and 8b.[23] However, high uncertainties in B and τ_{8a} resulted from such fits because the LIF intensity at relatively long decay times was low. τ_{8b} and τ were considered the same to within

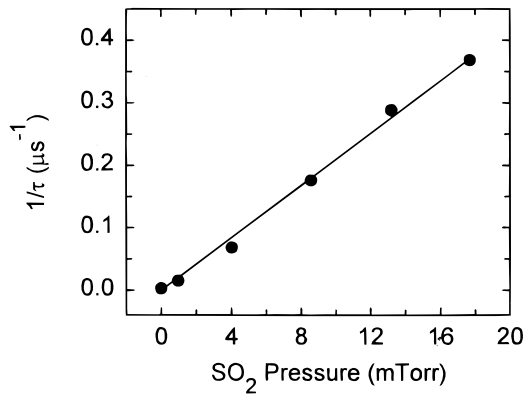

Figure 5. Plot for determining the second-order rate constant of Cr(a^5S_2) + SO_2. The conditions are the same as in Figure 4, except the partial pressures of SO_2 are changing. Each point represents an average of two to four measurements. The slope gives $k_{obs} = (6.49 \pm 0.12) \times 10^{-10}$ cm^3 molecule^{-1} s^{-1}, where the uncertainty represents $\pm 1\sigma$ in precision.

their combined experimental uncertainties. Thus, it was decided to use the results of eq 7. Figure 5 contains a plot of $1/\tau$ versus P_{SO_2} for Cr(a^5S_2) + SO_2 at 10 Torr total pressure. The slope gives $k = (6.49 \pm 0.12) \times 10^{-10}$ cm^3 molecule^{-1} s^{-1}, where the uncertainty represents $\pm 1\sigma$ in precision. The overall uncertainty is estimated at $\pm$35%. Rate constants for this reaction measured at 5 and 20 Torr total pressure are $k_{5Torr} = (6.05 \pm 0.08) \times 10^{-10}$ cm^3 molecule^{-1} s^{-1} and $k_{20Torr} = (6.40 \pm 0.21) \times 10^{-10}$ cm^3 molecule^{-1} s^{-1}, where the uncertainties represent precision. The averaged value is given in Table 2. Note that the value of this rate constant is larger than gas kinetic.

The temporal behavior of Cr(a^5D_0) in the presence of SO_2 was similar to Cr(a^5S_2). The other spin−orbit states of the Cr(a^5D_J) term exhibited exponential decay kinetics. The measured rate constant for this term in the presence of SO_2 is 2.97×10^{-10} ($\pm$30%) cm^3 molecule^{-1} s^{-1}.

Discussion

Photofragments. Mechanisms for the photodissociation dynamics of $Cr(CO)_6$ at 248 nm have been reported elsewhere,[18,19] and only a brief discussion as it applies to this work is given here. The production of Cr(a^7S_3), Cr(a^5S_2), and Cr(a^5D_J) requires two-photon dissociation processes at 248 nm. Other possible photodissociation products that could interfere with the decay kinetics of Cr(a^7S_3), Cr(a^5S_2), and Cr(a^5D_J) are other excited states of Cr formed from multiphoton processes, and unsaturated $Cr(CO)_x$, where $x = 1-5$. The growth observed at short times for Cr(a^7S_3) is likely due to the collisional quenching of excited Cr states. Excited states are not expected to radiate directly into the ground state over the course of 5−10 μs under multicollision conditions. Also, excited unsaturated chromium carbonyls are likely quenched instead of dissociating to Cr. In any event, significant feeding into the ground state is over in 1−10 μs, allowing measurements of the lifetimes of the ground state. No significant growth was observed for Cr(a^5S_2) and Cr(a^5D_J).

Cr(a^7S_3). The ground state, bimolecular channel

$$Cr + SO_2 \rightarrow CrO + SO \qquad \Delta H = 22.14 \text{ kcal mol}^{-1}\ ^{11} \quad (9)$$

is thermodynamically inaccessible at relatively low temperatures. Thus, adduct formation (eq 1) between Cr and SO_2 is the only viable channel, as observed. Adduct formation is exceptionally efficient in this system. The large values of the third-order rate and high-pressure rate constants, and the negative temperature dependence of the former indicate the absence of an energy barrier to adduct formation. The third-order rate constant is larger than those of other metal + small oxidant systems.[24−27] Such a large value of k_o indicates a tightly bound complex and a long-lived energized complex. To estimate the binding energy, E_b, of the $CrSO_2$ adduct relative to the ground-state reactants, simplified RRKM calculations using the formalism of Troe[14] were performed. In brief, the rate constant for the unimolecular dissociation of $CrSO_2$, k_{uni}, was first calculated. The limiting low-pressure third-order rate constant, k_o, was then calculated from the expression $K_{eq} = k_{uni}/k_o$ where K_{eq} is the equilibrium constant for the reaction $CrSO_2 \rightleftarrows Cr + SO_2$. The collision efficiency, β_C, of argon was taken as 0.20 in the calculations. K_{eq} was calculated using statistical mechanics methods. The binding energy of $CrSO_2$ was then adjusted until agreement was obtained between the calculated and experimental third-order rate constants.

The molecular parameters of $CrSO_2$ needed for estimating the value of K_{eq} were computed using the Spartan DFT suite of programs.[28,29] Calculations were performed at the NSLDA/BP86/DN* level.[13,28,29] These calculations are not meant to be exhaustive; instead, they serve mainly to provide reasonable estimates of the $CrSO_2$ molecular structure and vibrations. Several initial geometries and multiplicities were used. The septet state of the $\eta^2_{O,O}$ isomer was found to have the lowest relative energy; this isomer is of C_{2v} symmetry where the Cr atom is bonded to the two oxygen atoms. Vibrational harmonic frequencies were then calculated. Results of the calculations are given in the Appendix. It is worth mentioning here that at this level of theory, other isomers were found to lie within 30 kcal mol^{-1} of the septet $\eta^2_{O,O}$ isomer. This work is not meant to definitively assign a ground-state structure to $CrSO_2$. However, for the purposes of estimating the binding energy of $CrSO_2$, the lowest energy isomer at this level of theory is assumed to be the gas-phase reaction product.

Agreement between the calculated and experimental value of k_o at 297 K was obtained for $E_b = 53 \pm 3$ kcal mol^{-1}, where the uncertainty is based only on precision in the measured third-order rate constant. K_{eq}, and hence, E_b, is very dependent on the molecular structure of $CrSO_2$. Thus, E_b is offered only as a rough *estimate*. It is, however, a reasonable estimate. The binding energies of adducts formed between metal atoms (TM and main group) and O_2, SO_2, and NO are approximately 50 kcal mol^{-1}.[1,24−27]

The binding energies of $\eta^2_{O,O}$-type structures of $NaSO_2$ and KSO_2 adducts have been found to be approximately that of the corresponding metal-O_2 superoxides.[25,26] Similarly, low level DFT calculations gave a binding energy of $\eta^2_{O,O}$ $NiSO_2$ that is approximately equal to that of NiO_2.[1] It appears that $CrSO_2$ follows this trend. Martinez performed DFT calculations on CrO_2 and found that the lowest energy superoxide is a quintet with a binding energy of $\approx$52 kcal mol^{-1}.[30] Even though the superoxide is not the ground state determined by Martinez, the closeness of the binding energies of metal−O_2 superoxides and metal−SO_2 adducts suggests that the bonding is similar in these complexes; they have both ionic and covalent components to the bonding. The DFT ground state of CrO_2 is actually a C_{2v} triplet bent structure that has a binding energy of 125.6 kcal mol^{-1}; in this bent structure, the O−O bond is cleaved in favor of Cr−O bonding.[30] Parnis et al. also estimated the binding energy of CrO_2 from experimental kinetic data and simplified RRKM calculations.[31] Even though the structure of the product was uncertain, they obtained a binding energy of 113 kcal mol^{-1}

for the dioxide product, which is in good agreement with the DFT results. The superoxide gave binding energies greater than $\approx$60 kcal mol^{-1}.

The observed value of k_∞ at 297 K is approximately that of the hard-sphere collision rate constant of $k_{hs} = 2.3 \times 10^{-10}$ cm^3 molecule^{-1} s^{-1}.[20-22] The electron transfer mechanism (etm) cannot explicitly account for the value of k_∞. The rate constant is given by $k_{etm} = \sigma_{etm}\upsilon$, where σ_{etm} is the cross section for electron transfer and υ is the mean relative velocity of the colliders. σ_{etm} corresponds to the distance r_c at which the neutral potential energy curve of Cr + SO_2 crosses the potential energy curve of $Cr^+ + SO_2^-$, i.e.,

$$r_c = \frac{e^2}{4\pi\epsilon_o}\frac{1}{IP_{TM} - EA_{SO_2}} \tag{10}$$

where e is the electron charge, IP is the ionization potential, and EA is the electron affinity.[9] σ_{etm} is given by πr_c^2. Using tabulated values[9] of the ionization potential of Cr and the vertical electron affinity of SO_2 gives $k_{etm} = 1.0 \times 10^{-10}$ cm^3 molecule^{-1} s^{-1}, which is less than k_∞. This comparison implies that any electron transfer will take place after collision and that electron transfer is not as important in determining the rate of reaction as in a harpooning-type mechanism.

The only other reported association reaction between a TM and SO_2 is that of Ni and SO_2,[1]

$$Ni + SO_2 + M \rightarrow NiSO_2 + M$$
$$k_o = (3.3 \pm 0.3) \times 10^{-29} \text{ cm}^6 \text{ molecule}^{-2} \text{ s}^{-1}$$
$$k_\infty = (1.7 \pm 0.4) \times 10^{-10} \text{ cm}^3 \text{ molecule}^{-1} \text{ s}^{-1} \tag{11}$$

The above rate constants are at 296 K. The smaller k_o for Ni, compared to k_o for Cr, is attributed to Ni's $3d^84s^2$ ground-state electron configuration. It is worth mentioning that the ground state of Ni is influenced by the $3d^94s^1$ a^3D_3 at 205 cm^{-1}. In fact, these two states react with SO_2 at identical rates. For Ni, k_{hs} and k_{etm} are 1.9×10^{-10} and 7.2×10^{-11} cm^3 molecule^{-1} s^{-1}, respectively. Thus, the same argument above about the electron-transfer mechanism also applies here for Ni.

It is interesting to note that association reactions of Cr and other first row TM atoms with O_2 have been reported.[24,31] The efficiency of these reactions depend on the orbital occupancies of the TM atoms, with Cr reacting with O_2 most efficiently.

Cr (a^5S_2, a^5D_J). These excited states deplete quite efficiently in the presence of SO_2. The observation of some growth in ground-state Cr and the nonexponential decay kinetics of Cr(a^5S_2) and Cr(a^5D_0) indicate that physical quenching is an important exit channel for one or more Cr excited states. The production of CrO from Cr(a^5S_2) is approximately thermoneutral, and the production of CrO from the a^5D_J spin−orbit states is slightly exothermic.[11] Thus, O atom abstraction from these two Cr terms is also possible. A long-range attraction mechanism is operative for Cr(a^5S_2). $k_{etm} = 1.4 \times 10^{-10}$ cm^3 molecule^{-1} s^{-1}; thus, the simple electron transfer mechanism is not an adequate explanation. Another model that has been used successfully for metal + small oxidant systems is based on attractive dispersive forces that give interaction cross sections that are greater than σ_{etm}.[20,32] The rate constant, termed k_{C_6} here, is given by

$$k_{C_6} = \pi(2\epsilon/kT)^{1/3}\upsilon\Gamma(^2/_3) \tag{12}$$

where ϵ is the attractive potential between the colliders, k is the Boltzmann constant, T is the absolute temperature, υ is defined as above, and Γ is the gamma function. ϵ is taken as the C_6 coefficient for the attractive term in the Lennard-Jones 6-12 potential. For the Cr/SO_2 system, C_6 consists of two terms, a dipole−induced dipole term C_{ind} and a London dispersion attraction term C_{disp}. These terms are given by[33]

$$C_{ind} = \frac{\mu_{SO_2}^2\alpha_{Cr}}{(4\pi\epsilon_o)^2} \qquad C_{disp} = \frac{3}{2}\left(\frac{IP_{Cr}IP_{SO_2}}{IP_{Cr} + IP_{SO_2}}\right)\frac{\alpha_{Cr}\alpha_{SO_2}}{(4\pi\epsilon_o)^2} \tag{13}$$

where μ_{SO_2} is the dipole moment of SO_2,[9] α_{Cr} and α_{SO_2} are the polarizabilities of Cr and SO_2,[9] respectively, and ϵ_o is the permittivity in a vacuum. Polarizabilities of excited states are found to be larger than those for ground states. Thus, depletion rate constants for the excited states are expected to be larger than those for ground states. The value of α for Cr(a^5S_2) is taken as 14.5×10^{-24} cm,[3,34] and the IP was corrected for the excitation energy. Application of this model to Cr(a^5S_2) gives $k_{C_6} = 6.2 \times 10^{-10}$ cm^3 molecule^{-1} s^{-1}, which is in good agreement with the experimental value of 6.32×10^{-10} cm^3 molecule^{-1} s^{-1}. Long-range attractions are not important for the depletion of the a^5D_J spin−orbit states.

Group 6 TMs. This work on Cr + SO_2 completes an extensive study on the depletion of group 6 TM atoms by SO_2. Rate constants and other information for these reactions are summarized in Table 3. The third-order rate constant for the ground state of Cr is not listed because the other states do not deplete via a termolecular process. Also note that the listed k_{obs} for Cr(a^7S_3) represents the limiting high-pressure rate constant. k_{obs} for the other atoms and states are second-order rate constants. For comparison purposes, the hard-sphere collision rate constant is $\approx 2.1 \times 10^{-10}$ cm^3 molecule^{-1} s^{-1} for these systems. Only the ground states, a^5S_J states, and the highest energy spin−orbit states of the a^5D_J terms are listed (in general, all a^5D_J spin−orbit states behave similarly). Ground-state Cr reacts via an association reaction and ground-state Mo and W react via an abstraction reaction. The ground states of Cr and Mo have s^1 orbital occupancies and are reactive with SO_2, as shown by the values of k_o (in the results section) and k_{obs}. The ground state of W has an s^2 orbital occupancy and is relatively unreactive. This result is expected because of the s^2 orbital occupancy, i.e., the activation energy of W(a^5D_0) + SO_2, is likely due to promotion to an s^1 state.[5] Thus, the ground-state systems support the orbital occupancy argument, whether the reaction is termolecular or bimolecular.

Consider the group 6 a^5S_J states. These states have favorable electron configurations (s^1), and barriers to depletion are not observed, as expected. In fact, these states are all quenched efficiently by SO_2 with rate constants that are larger than gas kinetic (see Table 3). How does one account for the rapid depletion rates? The effective ionization potentials are less than the ground-state ionization potentials, thus making them more "prone" to interact via a harpooning-type mechanism. Note, however, that the rate constants in Table 3 calculated from the electron-transfer mechanism are less than the observed rate constants. The IPs of the TM atoms are too large for electron transfer to be rate determining. The "C_6" mechanism provides a better explanation for the depletion rates, as discussed above for Cr(a^5S_2). The calculated k_{C_6} values in Table 3 are reasonable in view of the experimental uncertainties in k_{obs} and approximations in the model. A detailed explanation on the quenching mechanism is complicated by the fact that chemical and physical quenching are possible depletion channels, and details of the potential energy surfaces are not known. One can conclude,

TABLE 3: Rate Constants for the Depletion of Group 6 Transition Metal Atoms by SO_2[a]

			k's (10^{-11} cm^3 molecule^{-1} s^{-1}) at ≈297 K[b]			
TM	energy (cm^{-1})	IP (eV)	k_{obs}[c]	k_{etm}	k_{C_6}	ref
Cr ($3d^5 4s^1$ a^7S_3)	0	6.77	27.3[d]	10	60	this work
Cr ($3d^5 4s^1$ a^5S_2)	7593.16	5.83	63.2	14	62	this work
Cr ($3d^4 4s^2$ a^5D_4)[e]	8307.57	5.74	29.7	15	62	this work
Mo ($4d^5 5s^1$ a^7S_3)	0	7.09	13	7.7	54	6
Mo ($4d^5 5s^1$ a^5S_2)	10768.22	5.76	38	13	56	6
Mo ($4d^4 4s^2$ a^5D_4)[f]	12346.31	5.56	18	14	56	6
W ($5d^4 6s^2$ a^5D_0)[g]	0	7.98	0.60	5.3	47	5
W ($5d^4 6s^2$ a^5D_4)[g]	6219.33	7.21	3.6	6.7	50	5
W ($5d^5 6s^1$ a^5S_3)	2951.29	7.67	40	5.9	50	5

[a] TM states and energies are taken from ref 12. Ionization potentials are taken from ref 9. [b] Rate constants were measured between 5 and 30 Torr total pressure in Ar buffer except for Cr(a^7S_3), which were measured in 5−500 Torr, Ar buffer. Uncertainties are ±30% except for Cr(a^5S_2) and Mo(a^5S_2) which are ±35% and ±50%, respectively. [c] The k_{obs} entries represent bimolecular rate constants except for Cr(a^7S_3). [d] k_{obs} is the limiting high-pressure second-order rate constant. [e] The k's for Cr(a^5D_{0-3}) are identical to those listed for the $J = 4$ state. The energies of this term range from 7750.78 to 8307.57 cm^{-1}. [f] The k's for Mo(a^5D_{1-3}) are identical to those listed for the $J = 4$ state. k_{obs} for the $J = 0$ state is ≈3×10^{-10} cm^3 molecule^{-1} s^{-1}. The energies of this term range from 10 966 to 12 346.31 cm^{-1}. [g] k_{obs} for this term ranges $(0.60-3.6) \times 10^{-11}$ cm^3 molecule^{-1} s^{-1}. The energies of this term range from 0 to 6219.33 cm^{-1}.

however, that these rates are controlled by long-range dispersion and dipole-induced forces, and they are entrance-channel controlled; i.e., the a^5S_J state is coupled directly to other TM states and/or TM oxides. The simple electron-transfer mechanism (harpooning in this case) does not account for the rapid rates of the a^5S_J states.

The depletion rate constants of the a^5D_J states are consistent with the electron-transfer mechanism. Cr(a^5D_J) and Mo(a^5D_J) deplete with little or no activation barriers, and W(a^5D_J) deplete with activation energies in the range 0.41−1.7 kcal mol^{-1}.[5] One way to test an electron transfer-type mechanism is to correlate the activation energies to the IPs. The large value of k_{obs} for Cr indicates the absence of any activation barrier. Using the Arrhenius equation to estimate the activation energy E_a of Mo gives $E_a \approx 0.3$ kcal mol^{-1} (A is taken as k_{hs}). E_a for W(a^5D_0) and W(a^5D_4) + SO_2 are 1.74 and 0.406 kcal mol^{-1}, respectively (the activation energies for the $J = 1$, 2, and 3 spin−orbit states are 1.00, 1.03, and 0.693 kcal mol^{-1}, respectively).[5] Thus, the activation energies correlate with the IPs. For Cr and Mo, all of the a^5D_J spin−orbit states deplete at the same rate, while there is some variation among the spin−orbit a^5D_J states of W. This observation is attributed to the energy spacings between the spin−orbit states; they are larger in W than in Cr and Mo. It is unlikely that the interconversions between the spin−orbit states of W will compete with the depletion rates.

The results presented allow us to conclude that the s^1 orbital occupancy is the primary factor in the *efficient* depletion of group 6 TM atoms by SO_2; i.e., depletion in which barriers are negligible. Long-range attractions influenced by dispersion forces and dipole−induced dipole forces allow the atoms to deplete at greater than collision rates, provided they are of s^1 orbital occupancy. Activation barriers may be present for states of s^2 orbital occupancy. These barriers depend on the IPs of the TM atoms, thus lending support for a contribution from an electron-transfer mechanism. Compared to other TM + small oxidant (O_2, CO_2, N_2O, NO) systems,[35] such a contribution is not unreasonable because the electron affinity of SO_2 is 1.107 eV, whereas the electron affinities of the other oxidants are less than 0.5 eV.[9]

The depletion kinetics of the group 6 TM atoms by SO_2 follow the same trend as for other TM/SO_2 systems. s^1 TM atoms deplete with little or no energy barriers, and some of them deplete with rates greater than gas kinetic. s^2 TM atoms deplete either at or below the collision rate. Nb + SO_2 is the only other system of s^1 orbital occupancy to have been reported.[3] The observed rate constant is 5.6×10^{-10} (±30%) cm^3 molecule^{-1} s^{-1}. The electron transfer mechanism predicts a rate constant of only 8.7×10^{-11} cm^3 molecule^{-1} s^{-1}, and the predicted C_6's value is 5.8×10^{-10} cm^3 molecule^{-1} s^{-1}. Thus, we conclude that the model based on long-range dispersion forces provides a better explanation for the fast depletion of s^1 TM atoms by SO_2 than the electron-transfer mechanism. To obtain a clearer picture on the association reactions of TM atoms with SO_2, falloff data are needed for other TM atoms. Once these data are obtained, correlations can be sought between rate parameters and atomic properties. A complete understanding of TM/SO_2 systems will no doubt be gained by accurate theoretical calculations.

Summary and Conclusions

SO_2 has been found to deplete the ground state and the first two excited terms of Cr very efficiently. Ground-state Cr reacts via a termolecular mechanism. The bond energy of the $CrSO_2$ adduct is estimated at ≈53 kcal mol^{-1} from combining low level DFT calculations and the kinetics results with RRKM calculations. The rate constant for Cr(a^5S_2) + SO_2 is greater than gas kinetic, and the a^5D_J term depletes at the collision rate. The Cr(a^5S_2) depletion rate is attributed to long-range attractions influenced by dispersion forces and dipole−induced dipole forces. Both physical and chemical quenching are likely for the excited terms. The depletion rate constants of Cr were compared to the depletion rate constants of the other group 6 TM atoms. It is found that the s^1 states are generally more reactive than the s^2 states, and the depletion of the s^2 states are influenced by an electron-transfer mechanism.

Acknowledgment. This research was supported by the Naval Academy Research Council and a Cottrell College Science Award of Research Corp.

Appendix

The DFT suite of SPARTAN programs[28,29] was used to calculate the molecular parameters of $CrSO_2$. Calculations were performed at the NSLDA/BP86/DN* level.[13,28,29] The septet $\eta^2_{O,O}$ isomer of $CrSO_2$ (C_{2v} geometry) gave the lowest energy. We found bond lengths of r(S−O) = 1.5625 Å and r(Cr−O) = 2.1636 Å. Bond angles are ∠(O−S−O) = 105.1973°, ∠(S−O−Cr) = 92.3922°, and ∠(O−Cr−O) = 70.0182°. Calculated frequencies, in units of cm^{-1}, are 147.09, 297.33, 305.37, 515.64, 899.93, and 910.34.

For the simplified RRKM calculations at 297 K, the threshold energy for dissociation E_o was taken as an adjustable parameter. E_o is equal to E_b because there is no barrier for adduct formation. The rate constant for the unimolecular dissociation in the low-pressure limit, k_{uni}, is given by[14]

$$k_o = \beta_C Z_{LJ} \frac{\rho(E_o)RT}{Q_{vib}} \exp(-E_o/RT) F_{anh} F_E F_{rot} F_{rot\ intn} F_{corr}$$

where β_C is the collision efficiency of Ar, Z_{LJ} is the Leonard-Jones rate constant, $\rho(E_o)$ is the vibrational density of states of $CrSO_2$ at E_o, F_{anh} is a correction for vibrational anharmonicity, F_E is a correction for the variation of the density of states, and F_{rot} is the molecular rotational correction factor. The corrections for the internal rotational modes and the coupling of the F factors, $F_{rot\ int}$ and F_{corr}, were taken as one.

A Lennard-Jones collision frequency of 6.42×10^{-10} cm^3 molecule^{-1} s^{-1} was calculated from reasonable values of the Lennard-Jones parameters.[22] β_c was taken as 0.20. $s = 6$ and $m = 3$.[14] $E_o = 53.3$ kcal mol^{-1}. Calculated RRKM parameters are $a(E_o) = 0.990$, $F_{anh} = 1.37$, $F_E = 1.05$, and $F_{rot} = 25.7$. Calculated K_{eq}, k_{uni}, and k_o values are 2.93×10^{-15} molecules cm^{-3}, 3.93×10^{-42} cm^3 molecule^{-1} s^{-1}, and 2.68×10^{-28} cm^6 molecule^{-2} s^{-1}, respectively.

References and Notes

(1) McClean, R. E. *J. Phys. Chem. A* **1999**, 103, 75.

(2) Campbell, M. L. *J. Chem. Soc., Faraday Trans.* **1998**, *94*, 1687.

(3) McClean, R. E.; Campbell, M. L.; Kolsch, E. J. *J. Phys. Chem. A* **1997**, *101*, 3348.

(4) Campbell, M. L.; Hooper, K. L.; Kolsch, E. J. *Chem Phys. Lett.* **1997**, *274*, 7.

(5) Harter, J. S. S.; Campbell, M. L.; McClean, R. E. *Int. J. Chem. Kinet.* **1997**, *29*, 367.

(6) McClean, R. E.; Campbell, M. L.; Goodwin, R. H. *J. Phys. Chem.* **1996**, *100*, 7502.

(7) Campbell, M. L.; McClean, R. E. *J. Phys. Chem.* **1993**, *97*, 7942.

(8) Herschbach, D. R. In *Advances in Chemistry and Physics*; Ross, J., Ed.; Interscience: New York, 1966; Vol. 10, Chapter 9.

(9) *CRC Handbook of Chemistry and Physics*, 75th ed.; Lide, D. R., Ed.; CRC Press: Boca Raton, FL, 1995.

(10) See, for example: Hamrick, Y. M.; Taylor, S.; Morse, M. D. *J. Mol. Spectrosc.* **1991**, *146*, 274.

(11) Chase, M. W., Jr., Ed. *NIST-JANAF Thermochemical Tables*, 4th ed.; *J. Phys. Chem. Ref. Data* **1998**, Monograph 9.

(12) Moore, C. E. *Atomic Energy Levels as Derived from the Analysis of Optical Spectra*; Natl. Stand. Ref. Data Ser.; U.S. Natl. Bur. Stand.: Washington, DC, 1971; NSRDS-NBS 35.

(13) *Modern Density Functional Theory: A Tool for Chemistry*; Seminario, J. M., Politzer, P., Eds.; Elsevier: New York, 1995.

(14) Troe, J. *J. Phys. Chem.* **1979**, *83*, 114.

(15) Akhmadov, U. S.; Zaslonko, I. S. *Kinet. Catal.* **1988**, *29*, 808.

(16) Campbell, M. L.; McClean, R. E. *J. Chem. Soc., Faraday Trans.* **1995**, *91*, 3787.

(17) Martin, G. A.; Fuhr, J. R.; Wiese, W. L. *J. Phys. Chem. Ref. Data* **1988**, *17* (Suppl. 3).

(18) Tyndall, G. W.; Jackson, R. L. *J. Chem. Phys.* **1988**, *89*, 1364.

(19) Venkataraman, B.; Hou, H.-q.; Zhang, Z.; Chen, S.; Bandukwalla, G.; Vernon, M. *J. Chem. Phys.* **1990**, *92*, 5338 and references therein.

(20) Smith, I. W. M. *Kinetics and Dynamics of Elementary Gas Reactions*; Butterworth: London, 1980; Chapter 3.

(21) Fischer, C. F. *The Hartree−Fock Method for Atoms*; Wiley: New York, 1977.

(22) Reid, R. C.; Prausnitz, J. M.; Poling, B. E. *The Properties of Gases and Liquids*, 4th ed.; McGraw-Hill: New York, 1987.

(23) Campbell, M. L.; McClean, R. E.; Harter, J. S. S. *Chem. Phys. Lett.* **1995**, *235*, 497.

(24) Brown, C. E.; Mitchell, S. A.; Hackett, P. A. *J. Phys. Chem.* **1991**, *95*, 1062 and references therein.

(25) Shi, Y.; Marshall, P. *J. Phys. Chem.* **1991**, *95*, 1654.

(26) Goumri, A.; Laakso, D.; Rocha, J.-D. R.; Francis, E.; Marshall, P. *J. Phys. Chem.* **1993**, *97*, 5297.

(27) McClean, R. E.; Campbell, M. L.; Vorce, M. D.; Medhurst, L. J. *J. Phys. Chem. A* **1999**, *103*, 2659.

(28) *SPARTAN*; Wavefunction, Inc.: Irvine, CA, 1997.

(29) Hedre, W. J.; Lou, L. *A Guide to Density Functional Calculations in SPARTAN;* Wavefunction, Inc.: Irvine, CA, 1997.

(30) Martinez, A. *J. Phys. Chem. A* **1998**, *102*, 1381.

(31) Parnis, J. M.; Mitchell, S. A.; Hackett, P. A. *J. Phys. Chem.* **1990**, *94*, 8152.

(32) Vinckier, C.; Helaers, J.; Christiaens, P.; Remeysen, J. *J. Phys. Chem. A* **1999**, *103*, 11321.

(33) McQuarrie, D. A.; Simon, J. D. *Physical Chemistry, A Molecular Approach*; University Science Books: Mill Valley, CA, 1997; Chapter 16.

(34) The value of α chosen here is 1.25 times the tabulated value for ground-state Cr, which gives a value that is equal to the upper limit for α of the ground state. (The estimated accuracies of the polarizabilities for ground-state TM atoms is 25%.[9]) This approach is taken in case α changes very little for the excited states. In any event, α is not expected to increase significantly for a change in spin.

(35) Honma, K.; Clemmer, D. E. Laser *Chem.* **1995**, *15*, 209.